Three-Dimensional Flow and Thermal Structures in Glass Melting Furnaces. Part I. Effects of the Heat Flux Distribution. Glass Science and Technology, Vol. 75, No.2 pp. 55-68.

Laurent Pilon, Guochang Zhao, and Raymond Viskanta

Heat Transfer Laboratory
School of Mechanical Engineering
Purdue University
West Lafayette, IN 47907, USA

Phone: (765)-494-5632
Fax: (765)-494-0539
E-mail: viskanta@ecn.purdue.edu

January 15, 2006

ABSTRACT

This paper presents a study of the flow and thermal structures in the molten glass bath of a typical glass melting furnace with a throat but without air bubblers or electric boosting. Different separate effects on the flow structure of the glass melt are simulated, but only the glass melt is considered. The net heat flux distribution is imposed at the combustion space/glass melt interface, and its effects on the flow and thermal structures of the glass melt are analyzed in a systematic manner by changing the heat flux distribution while keeping the total heat input to the glass bath constant. The main purpose of the work is to evaluate the capability of the furnace operators to control the glass flow and temperature fields by adjusting the firing in the combustion space. The physical phenomena affecting the flow structure in the glass melt are analyzed and discussed in detail. The major results of the study indicate that (i) the heat flux distribution has no significant effect on the flow structure of the glass melt under the batch blanket where several Rayleigh-Benard cells develop in the spanwise direction, (ii) a heat flux gradient in the longitudinal direction is required to generate two recirculation loops in the direction, and (iii) steep heat flux gradient in the refining part of the tank increase significantly the size of the refining recirculation loop near the front wall.

NOMENCLATURE

c	Specific heat
ΔH_{melt}	Total enthalpy of melting of the batch
g	Specific gravity
h	Depth within the glass melt
$\vec{i}, \vec{j}, \vec{k}$	Unit vectors in the physical space
k	Thermal conductivity
L_b	Length of the batch blanket
L_{max}	Longitudinal location of the maximum heat flux
L_0	Longitudinal location of the zero heat flux
$\dot{m}_b$	Batch mass flow rate
$\dot{m}_{pull}$	Glass mass flow rate at the throat
p	Pressure
q''	Heat flux
q''_0	Heat flux at the back wall (x = 0 m)
$q^*(y)$	Dimensionless multiplying factor of the heat flux
$Q'_{melt \rightarrow batch}$	Heat transfer rate from the glass melt to the batch per unit length of batch
$\dot{S}$	Volumetric heat source
T	Temperature
T_0	Reference temperature
t	Time
u	Velocity vector in the x-direction
v	Velocity vector in the y-direction
$\vec{v}$	Velocity vector
w	Velocity vector in the z-direction
W	Glass tank width
x	Longitudinal location (see Figure 3)
y	Spanwise location (see Figure 3)
z	Local depth within the glass melt (see Figure 3)
Greek symbols	
α	Thermal diffusivity
β	Thermal expansion coefficient
ρ	Density
μ	Dynamic viscosity
ϕ	Local volumetric gas fraction
Subscripts	
b	Refers to the batch
$bubbles$	Refers to the depth under the batch where bubbles are present

eff	Refers to effective values
max	Refers to the value at L_{max}
$melt$	Refers to the melting of the batch
sub	Refers to the submerged part of the batch

INTRODUCTION

Two different types of glass melting furnaces are commonly used in the glass industry [1]:

1. *Float glass furnaces* are often open cross-fired regeneration furnaces consisting of melting and conditioning regions connected by a waist. The bottom of the tank is often stepped. This type of furnaces is fairly large and used to produce large quantity of glass products such as flat glass sheets.

2. *Submerged throat furnaces* are used, for example, to produce glassware, container glass, and TV panels and funnels. They consist of a melting tank and a working section connected by a channel or throat.

The introduction of the batch into the furnace can be either from the back wall in the longitudinal direction or from the sides by using different types of chargers. The resulting batch coverage can assume many different shapes from a uniform blanket to dispersed batch logs floating at the surface of the glass melt. Moreover, the glass tank can be equiped with electric boosters or bubblers to increase the temperature uniformity and the refining of the glass melt. Many design parameters and operating conditions should also be considered in the combustion space for example: (i) the fuel (natural gas, fossil fuel or coal), (ii) the oxidizer (air or commercial grade oxygen), (iii) the shape of the flame, and (iv) the regeneration.

Thanks to the development of numerical methods (in particular, finite-difference methods [2]) and the increases in both computing speed and capacity, computer simulations of glass melting furnaces have been the object of intensive research over the last two decades [2, 3]. Computer simulations provide valuable alternatives and supplemental tools to (a) direct observations and measurements in actual furnaces and (b) physical models, for improved design and control of glass melting furnaces [2,3]. Early numerical simulations were based on two-dimensional models due to very limited computer resources [3]. However, two-dimensional models that treat only the glass flow in the longitudinal direction were soon proven to be inadequate [2, 3], and three-dimensional calculations were presented as early as 1972 [2]. Two-dimensional studies of the flow and thermal structure in the glass melting tank can still be found in recent literature [4–6]. Even though the issues raised in these recent publications are of fundamental interest, the resulting conclusions drawn should be used with great caution for operating glass melting furnaces.

The present study as well as the following literature review are restricted to the flow and thermal structures in the molten glass bath of a typical glass melting furnace with a throat but without air bubblers or electric boosting. This study aims at improving the understanding of physical phenomena affecting the flow structure in the glass melt. The results are of significant importance in improving the furnace performances in term of glass quality and energy efficiency.

LITERATURE REVIEW

The flow patterns in glass melting furnaces with a throat are believed to feature two circulations loops in the longitudinal direction as shown in Figure 1. The flow starting under the batch, circulates between the two circulation loops. The glass melt flows downward along the back wall under the first circulation loop and rises to the glass surface between the two loops. Then, it flows downward along the front wall and around the second circulation loop and finally exits through the throat. This flow pattern was confirmed by a two-dimensional numerical simulation [7]. However, Zhiqiang and Zhihao [1] did not experimentally observed such an ideal flow pattern. Instead, they observed that a part of the pull current flows directly from under the batch along the bottom of the glass tank to the throat as shown in Figure 2. Thus, the quality of the product is degraded due to a shorter residence time of the glass melt in the tank. The authors suggested the use of the LoNOx melter design developed by Sorg Company or the use of air bubblers as possible solutions to the degradation of the glass quality [1].

Curlet *et al.* [8] performed experiments using a physical model to simulate the flow patterns in glass

melting furnaces. The batch was simulated by a copper plate cooled with water to maintain the surface of the model fluid (glycerol) at constant temperature. The side and end walls were cooled to simulate the heat losses and electrical heaters where located above the free surface to produce a uniform heat flux. The authors identified local convective instabilities under the simulated batch similar to the Rayleigh-Benard instabilities caused by the fact that the liquid at the simulated batch/glass melt interface is heavier than that present at the bottom of the tank. The roll cells tend to enhance heat transfer from the model fluid in the bath to the batch leading to lower fluid temperatures [8]. A companion two-dimensional code that accounts for the three-dimensional effects by using a source-sink method was also developed. Good agreement with experimental data was found. The presence of Rayleigh-Benard type instabilities was confirmed by Ungan and Viskanta [9] who used a three-dimensional model of the glass bath. More recently, Lim *et al.* [4] showed numerically that the flow under the batch blanket become oscillatory and even chaotic. However, their boundary conditions were highly idealized. For example, they used two different uniform and constant temperatures at the glass melt/combustion space interface as well as at the glass melt/batch interface, and the tank walls were assumed to be adiabatic. First, the assumption that the temperature at the free glass surface is constant is not realistic since a hot spring is required and is typically used to produce two recirculation loops in which the glass particles become trapped and increase the residence time of the glass melt in the tank to improve homogenization of the melt and to enhance glass quality.

Finally, the effects of the heat losses from the side walls and bottom, the bath depth, and the surface boundary conditions in a glass tank in an absence of pull were presented by Ungan and Viskanta [10]. They demonstrated that the sidewall heat losses were very effective in enhancing the cells under the batch. Moreover, Ungan and Viskanta [10] showed that the losses at the bottom are "capable of amplifying or reducing the strength of the cells by regulating the average temperature and thus the viscous force within the melt". The tank depth was also proved to have a significant impact on the arrangement of the cells under the batch [10]. They also concluded that two-dimensional models are incapable of simulating the heat losses from the sidewalls and thus overpredict the temperature close to the sidewalls. However, at the centerline the results obtained by two-dimensional models compare well with their three-dimensional counterparts. This can be attributed to the relatively weak secondary circulation cells near the sidewalls where the velocities are too small to create any significant change in the longitudinal flow direction [1].

There exists a strong coupling between combustion space, melting of the batch, and glass melt. Numerous studies have presented interactive models to account for the coupling between each component [9, 11, 12]. However, the aim of the present work is to study separate effects on the flow structure of the glass melt; therefore, only the glass melt is considered and a net heat flux distribution is imposed at the combustion space/glass melt interface; its effects on the flow and thermal structures in a model melting tank are analyzed in a systematic manner. The choice of imposing a heat flux distribution instead of the glass surface temperature [10, 13–15] is based on the fact that in actual glass melting furnaces, the furnace operators can choose the fuel firing pattern and thus impose the heat flux distribution, while they have no direct control over the glass melt surface temperature.

MATHEMATICAL FORMULATION

Figure 3 shows a schematic of a model glass melting tank and the system of coordinates used in this study. A brief description of the model assumptions and of the governing equations follows and details can be found elsewhere [2, 11]. In the present study only the glass melt is considered. The heat flux distribution from the combustion space to the batch/glass melt is imposed. A simple energy balance on the batch was made to insure the energy conservation was satisfied for a given batch length.

Model Assumptions and Governing Equations

The analysis uses the following simplifying assumptions [2]:

1. The molten glass is incompressible, homogeneous, and Newtonian fluid;
2. The molten glass flow is laminar;
3. Variation of glass composition along the tank is neglected, i.e., evaporation of volatile species from the glass surface and the presence of gas bubbles on the thermophysical properties and radiation

characteristics of glass melt is not considered;

4. The radiation from the combustion space to the glass melt and to the batch and from the glass melt to the batch is treated as a diffusion process, i.e., the glass and the batch are optically thick and the Rosseland approximation is valid;

5. The Boussinesq approximation is valid, i.e., the density is a linear function of temperature;

6. The glass melt surface is horizontal;

7. Rheology and chemical reactions in the batch and foam formation are neglected;

8. Coupling between the batch blanket and the glass melt in the tank is weak, i.e., the interaction between the complex physicochemical processes in the batch and the glass tank is only through mass and energy balances at the flat batch/glass melt interface;

Some of the above simplifying assumptions are well justified, while others are questionable but have been made to simplify the governing equations. For example, the presence of sand grains and bubbles in the glass melt affect the radiative characteristics and the thermophysical properties of the glass melt. However, little quantitative information is known about the effects of such impurities on the radiative heat transfer. More recently, Cheong *et al.* [16] questioned the treatment of radiative heat transfer as a diffusion process and showed that such an approximation is not adequate when the depth of the glass layer is less than 0.5 m. Instead, they suggested the use of the P-1 approximation not only for shallow but also for deep glass baths. The diffusion approximation, however, appears to be satisfactory in the present analysis dealing with a glass bath more than 1 m deep.

Using the above simplifying assumptions, the model equations can be expressed as follows:

$$\nabla \vec{v} = \vec{0} \tag{1}$$

$$\rho(\vec{v} \cdot \nabla)\vec{v} = \nabla(\mu \nabla \vec{v}) - \nabla(p) + \rho g \beta (T - T_0) \tag{2}$$

$$\rho c(\vec{v} \cdot \nabla)T = \nabla \cdot (k_{eff} \nabla T) + \dot{S} \tag{3}$$

where ρ, $\vec{v}$, T, and p denote the density, velocity, temperature, and pressure of the glass melt, respectively. The volumetric heat sources $\dot{S}$ can be found in the literature [10, 17]. Note that all the thermophysical properties except the density depend on the temperature. This dependence on temperature makes the simulation more complex, and the use of a consistent set of thermophysical properties for a given type of glass melt is of major importance if one wants to obtain realistic predictions of the flow structure in the glass melt.

The melting of batch raw materials is a complex physicochemical process which involves a large number of chemical reactions and phase transformations occurring over the wide temperature range from 1000 to 1500 K [18]. Thus, the melting of the batch cannot be treated as a normal change of phase from solid to liquid. In order to model the melting process, a constant temperature (called melting temperature and noted T_{melt}) was imposed at the batch/glass melt interface, corresponding to the minimum temperature at which a clear glass is obtained. Even though, the melting of the batch is not modeled, the overall energy balance for the batch blanket was satisfied:

$$Q'_{melt \to batch} L_b + \int_0^{L_b} q''(x) W \, \mathrm{d}x = \dot{m}_{pull} \Delta H_{melt} \tag{4}$$

where $Q'_{melt \to batch}$ is the heat transfer rate from the glass melt to the batch per unit length of the batch. The heat flux from the combustion space to the surface of the glass melt is $q''(x)$, W is the width of the tank, L_b is the batch length, and ΔH_{melt} is the enthalpy per unit mass of molten glass required to obtain clear glass at the melting temperature T_{melt} from raw batch at 320 K. Finally, $\dot{m}_{pull}$ is the pull rate, i.e., the total mass of glass exiting the furnace per unit of time. The determination of $Q'_{melt \to batch}$ requires several iterations. However, we found that its value does not change significantly from one calculation to another, and in all cases it represents about 10% of the total heat input required to melt the batch; the other 90% come from the combustion space. For the conditions of the present study, a good approximate value for $Q'_{melt \to batch}$ is 3×10^6 W/m.

Boundary Conditions

Thermal Boundary Conditions

The batch coverage as well as the heat flux from the combustion space to the batch and the glass melt free surface are assumed to be known. The heat losses through the refractory walls are estimated based on conduction through the different layers of the refractories and with cooling of the wall by natural convection to air at ambiante temperature and radiation to the surroundings at a constant temperature. The temperature at the batch/glass melt interface is assumed to be the minimum temperature at which clear glass is obtained by heating the raw batch initially at room temperature.

Velocity Boundary Conditions

The velocity boundary conditions were as follows:

$$\vec{v} = \vec{0} \qquad \text{at the glass melt/wall interface} \tag{5}$$

$$\vec{v} = u_b(x)\vec{i} \qquad \text{at the batch/glass melt interface} \tag{6}$$

$$\vec{v} = u\vec{i} \qquad \text{and} \qquad \frac{\partial u}{\partial z} = 0 \qquad \text{at the glass free surface} \tag{7}$$

$$\vec{v} = u(y)\vec{i} \qquad \text{and} \qquad \frac{\partial u}{\partial x} = 0 \qquad \text{at the throat} \tag{8}$$

Based on the observations that unlike float glass furnaces, no back flow occurs from the working end to the melting tank in furnaces with a submerged throat owing to the narrowness of the throat [1], a no-slip boundary conditions at the throat was imposed by Equation (8) as recommended by Patankar [19].

The batch blanket is assumed to have a uniform x-direction velocity across the width of the tank but varying with the longitudinal direction. The other boundary conditions are commonly used in the literature [11] and need not be discussed further.

Thermophysical Properties

Appropriate specification of the thermophysical properties is a major concern in modeling of glass melting furnaces [20, 21]. Up to now, no reported simulation of glass melting furnaces has used a consistent set of thermophysical properties for a given glass melt. The purpose of this work is neither to develop an extensive database nor to provide new experimental results or measurement methods. Instead, it aims at collecting and assessing the available data concerning soda-lime silicate glass. Soda-lime silicate glass is the most widespread and inexpensive form of glass used to manufacture many different products such as containers, windows, lamps, lenses, etc. [22, 23]. Particular attention was paid to the thermophysical properties of the most common composition [74 SiO_2-16 Na_2O-10 CaO (mol.%)] soda-lime silicate glass or very similar compositions over the temperature range of 1000 to 2000 K.

Density and Thermal Expansion Coefficient

The density depends on the glass composition, the temperature, and the prior history [24]. In the present study, only the two first parameters are considered. The change of the glass density with temperature is approximated by

$$\rho(T) = \rho_0[1 - \beta(T - T_0)] \qquad \text{in kg/m}^3 \tag{9}$$

where ρ_0 is the density of the melt at T_0 and β the linear coefficient of expansion.

The thermal expansion is not only of interest for the usage of glass products but also for the calculation of the gravity driven flow of the glass melt [11]. Thermal expansion coefficient is strongly dependent on the glass composition [23–25]. Analysis of data reported by Coenen [25] leads to a thermal expansion coefficient of 6.59×10^{-5} K^{-1} for 73.8 SiO_2-15.5 Na_2O-10.7 CaO (mol.%) soda-lime silicate glass. Then, Equation (9) becomes

$$\rho(T) = 2406.5[1 - 6.59 \times 10^{-5}(T - 1123.15)] \qquad \text{in kg/m}^3 \tag{10}$$

The variation of the glass density in the temperature range of interest is very small: the density decreases only by 6.5% from 1000 K to 2000 K; therefore the glass density will be considered as a constant in the computations except for the calculation of the gravity driven flow of the glass melt for which the Boussinesq's assumption is used.

Dynamic Viscosity

The viscosity of soda-lime silicate glass is strongly dependent on the temperature and less strongly on the glass composition [24]. According to Lakatos *et al.* [24, 26], the dynamic viscosity of 74 SiO_2-16 Na_2O-10 CaO (mol.%) soda-lime silicate glass can be expressed as

$$\mu = 4.448 \times 10^{-3} exp\left[\frac{8982}{T - 539.4}\right] \qquad \text{in Pa s} \tag{11}$$

Moreover, it has been shown that the water vapor dissolved in the glass melt greatly lowers its dynamic viscosity at low temperatures (between 1250 and 1450 K) [24]; at higher temperatures the effect of water vapor on the glass melt viscosity is very small [24, 27] and will be neglected in the present study.

In the above expressions, neither the density of the melt ρ nor its dynamic viscosity μ depends on the volume fraction of gas bubbles present in the melt since we assumed that bubbles had no effect on the thermophysical properties of the melt. However, if the local gas void fraction in the melt is sufficiently large the density of the mixture decreases and its viscosity increases due to the resistance of the bubbles to the deformation of the flow field caused by their presence [28]. If one wants to consider the effect of the bubbles on the thermophysical properties of the melt, one has to compute simultaneously the thermal flow field of the glass melt and the bubble population balance equation. This calculation is very time consuming and requires significant computational resources; therefore, it will not be considered further.

Specific Heat

Sharp and Ginther [29] studied the effect of temperature and composition on the mean specific heat c_p of soda-lime silicate glasses. They observed that the specific heat varies slightly with glass composition [30] and for 74 SiO_2-16 Na_2O-10 CaO (mol.%) soda-lime silicate glass they proposed the following expression,

$$c(T) = \frac{2.18667T + 138.12}{0.00146T + 0.6012} \qquad \text{in J/kgK} \tag{12}$$

One can notice that the specific heat does not vary significantly over the temperature range of 1000 to 2000 K. Therefore, in the rest of this study the specific heat will be taken as constant and equals to its average value between 1000 and 2000 K, i.e., $c = 1231 J/kgK$. This assumption leads, at most, to an error of 5%.

Thermal Diffusivity and Effective Conductivity of the Melt

The thermal diffusivity α of the glass melt is an important thermophysical property for the thermal flow calculation in the glass melt as well as for the calculation of bubble generation and transport. Van Zee and Babcock [31] reported data for 72.6 SiO_2-14 Na_2O-13.4 CaO (mol.%) soda-lime silicate glass over the temperature range of 1000 to 1700 K. The second order polynomial fitting the experimental data using the least square method can expressed as

$$\alpha(T) = 6.8765 \times 10^{-5} - 1.1948 \times 10^{-7} T + 5.3816 \times 10^{-11} T^2 \qquad \text{in m}^2\text{/s} \tag{13}$$

From the experimental thermal diffusivity data and knowledge of the specific heat and the density, an expression for the effective thermal conducitivity k_{eff} of the glass melt can be obtained as:

$$k_{eff}(T) = \frac{\alpha(T)}{\rho c} = 213.0 - 0.3698T + 1.658 \times 10^{-4} T^2 \qquad \text{in W/mK} \tag{14}$$

Note that the effective conductivity k_{eff} accounts for both conduction and radiation heat diffusion in the molten glass.

Numerical Solution Method

The system of equations is discretized by finite-difference techniques using staggered grids for the scalar variables and for the vector variables. The resulting system of finite-difference equations is solved numerically using the SIMPLER algorithm [19]. The details of the solutions scheme are given elsewhere [11] and not need to be repeated here. The governing equations were solved by iteration until the mass and energy balances for the glass melt were satisfied. Testing the grid independency in the x- and z-directions was not judged necessary based on similar previous work [9] and on the flow pattern observed. Indeed, two large circulation

loops appear in the longitudinal direction and 66 grid points in the x-directions and 25 in the z-direction appeared to be sufficient to capture the flow structure. On the other hand, numerous Rayleigh-Benard cells can appear in the spanwise direction of the tank and a grid sensitivity study in the y-direction was required. Three different grids sizes ($66 \times 21 \times 25$, $66 \times 39 \times 25$, $66 \times 78 \times 25$) were considered and it was found that the grid of $66 \times 39 \times 25$ provides a good compromise between computer time required and the resolution needed to resolve details of the flow field of the molten glass.

RESULTS AND DISCUSSION

Model Glass Tank and Parameters

The tank considered was 15.85 m long, 7.315 m wide, and 1.03 m deep (see Figure 3). The molten glass exits the tank through a throat located at the bottom and in the middle of the front wall and having a cross-sectional area of (0.386×0.802) m^2. The raw material leading to a glass melt of composition of 74 SiO_2-16 Na_2O-10 CaO (mol.%) is introduced into the tank at a rate $\dot{m}_b$ of 356 tons/day (or 4.12 kg/s) in the form of a loose blanket covering the entire width of the tank. Since about 200 kg of gases are produced per ton of batch introduced [32], the corresponding glass production rate $\dot{m}_{pull}$ is 297 tons/day (or 3.347 kg/s) of molten glass.

Madivate [33] presented experimental data for the energy ΔH_{melt} required to bring the batch from room temperature to clear molten glass. The value of 2200 kJ/kg for glass of compositions similar to that of interest in the present work was used. The value of ΔH_{melt} corresponds to a glass composition of 74 SiO_2-16 Na_2O-10 CaO (mol.%) and melting temperature T_{melt} of 1450 K. Moreover, the batch blanket was assumed to float at the surface of the molten glass without being submerged.A linear decrease of the glass melt velocity at the batch/glass melt interface from 0.2 cm/s where the batch enters the furnace to zero at the tip of the batch blanket was chosen to simulate the fact that the batch blanket becomes thinner and less compact from the loading zone to the tip. The maximum velocity of 0.2 cm/s was computed based on the pull rate of 4.12 kg/s for a batch blanket covering the entire width and having a density of 1400 kg/m^3 and a thickness of 20 cm.

The heat losses between the glass melt and the ambient surroundings through the walls were computed assuming 1-D heat conduction through the refractories and cooling of the walls by natural convection using an ambiant temperature of 320 K. The construction of the sidewall refractories were considered to be the same, with an overall heat transfer coefficient of 3.86 W/m^2K. At the bottom of the tank the overall heat transfer coefficient equals 3.89 W/m^2K and that at the back and front wall is equal to 5.57 W/m^2K.

The heat flux incident from the combustion space and reaching the surface of the batch and of the molten glass is assumed to have the longitudinal profile shown in Figure 4, where the parameters q''_{max} and q''_0 are the maximum heat flux and the heat flux at the back wall (x = 0 m), respectively. L_{max} and L_0 are the distances from the back wall to the location of the maximum heat flux and to that where the heat flux vanishes, respectively. Such a heat flux profile was chosen based on industrial practices. The intent is to create a hot spring forcing the glass melt to circulate in two recirculation loops in the longitudinal direction (see Figures 1 and 2). The glass melt parcels and the impurities (unmelted sand grains and bubbles) tend to be trapped in the recirculation loops allowing the refining and homogenization processes to take place. Note also that the heat flux distibution presented in Figure 4 feature a negative heat flux close to the front wall. In this region of the tank, the glass surface is cooled by transferring energy to the combustion space.

The present study presents an original contribution to the understanding of the different design and operating parameters in glass melting furnaces. First, the baseline case is defined and studied in details. Then, the effects of several operating parameters describing the heat flux distribution from the combustion space to the glass surface that can be adjusted by a furnace operator in a simple manner are discussed. Particular attention is paid to:

1. The uniformity of the net heat flux from the combustion space to the glass melt
2. The location of the zero heat flux L_0
3. The location of the maximum heat flux L_{max}
4. The presence of a foam layer

5. The shape of the heat flux in the spanwise direction characterized by the multiplying factor $q^*(y)$

Table 1 summarizes the conditions prescribed in the different simulations presented and discussed in the following sections.

Baseline Case

The baseline case was chosen based on typical conditions previously simulated in the literature [4, 5, 10]. It serves as a reference around which the parameters of interest are varied and is defined by the following parameters:

(i) The length of the batch blanket L_b was arbitrarily taken as 6.5 m, based on previously reported simulations [14] and on the two-dimensional study by Lim *et al.* [5] who showed that the batch blanket should cover between 25 to 40% of the glass surface for an optimum melting rate. The inlet temperature of the batch is taken as 320 K.

(ii) The location of the maximum heat flux q_{max} was chosen 1 m away from the tip of the batch, while the zero heat flux is located 2 m away from the front wall, i.e., $L_0 = 13.84$ m.

(iii) For all the simulations the total energy transferred from the combustion space to the glass melt was maintained to a constant value of 8.3 MW. Then, assuming that the heat flux at the back wall (x = 0 m) equals half the maximum heat flux, the maximum heat flux q''_{max} satisfying the batch energy balance equation [Equation (4)] equals 133.92 kW/m^2.

Figure 5 shows the velocity and temperature profiles as well as the "streamtraces" at the tank centerline. The streamtraces shown are the streamlines plotted in the two-dimensional vector field obtained by projecting the three-dimensional vector field onto the cross-section of interest. For example, the streamtraces in the x-z plane are the streamlines constructed from the u- and w-components of the velocity field. The range of temperatures seems to be in agreement with previous published results [14] and with experimental measurements reported for operating furnaces [34]. One can observe the predominance of the flow in the longitudinal direction. For the tank considered, the ideal flow pattern described in Figure 1 is not predicted. Instead, the experimental observations by Zhiqiang and Zhihao [1] on the flow pattern in the longitudinal direction are confirmed, i.e., a part of the pull current goes directly from under the batch to the throat. The flow pattern described by Ungan and Viskanta [10] for a tank without glass outflow is not observed in the the simulations performed, the largest descrepancies occur close to the front wall. This indicates that the pull of the glass at the throat can strongly affect the flow pattern in the region close to the exit and the deflections of the streamtraces near the throat are apparent in Figure 5.

Sixteen Rayleigh-Benard cells can be observed under the batch in the spanwise direction as shown in Figure 6 for x = 3.5 m. The sixteen cells extend along the entire length of the batch but disappear as soon as the glass surface is in direct contact with the combustion space. From the tip of the batch to the location of the zero heat flux, only two cells develop in the two bottom corners of the tank as shown in Figure 6 at x = 7 and 10 m. The combination of the heat losses through the sidewalls and through the bottom of the tank create temperature gradients in the lateral direction in the vicinity of the bottom corners that generate the cells. In the vicinity of the front wall, at x = 13 m and 15 m, a total of four cells develop in each corner of the cross-section (see Figure 6). The two cells forming at the surface of the glass melt are due to the heat losses through the front wall, the sidewalls, and to the combustion space as the negative heat flux increases. On the other hand, the cells forming at the bottom corners are due to the combination of the heat losses through the bottom, the sidewalls, and the front wall. As one moves closer to the front wall, the heat losses to the combustion space increase, the cells forming at the surface of the glass melt grow and extend deeper into the tank while those at the bottom corners seem to be damped by the outflow at the throat (see evolution from x = 10 m to x = 15 m in Figure 6).

A word of caution should be mentioned here: the streamtraces plotted in all the figures should not be confused with pathline or streamlines of glass particles in three dimensions. Instead, they are plotted in two-dimensions onto the plane of projection. In regions where the flow is highly three-dimensional such as under the batch or close to the front wall, streamtraces should be seen as a simple way to visualize the flow structure and how each component of the velocity vector behaves.

Uniform Heat Flux Distribution

The simplest case consists of imposing a uniform net heat flux from the combustion space to the glass surface. For a total constant heat input of 8.3 MW, a uniform net heat flux of 71.65 kW/m^2 is imposed. Figure 7 shows the velocity, temperature fields and the streamtraces at the centerline when a uniform heat flux is imposed at the surface of the glass melt. One can see that only one recirculation loop in the longitudinal direction develops. One can see that the isotherms in the refining part of the tank where the glass is in direct contact with the combustion space are parallel to the glass free surface, as if a constant temperature was imposed at the glass/combustion space interface. Due to the uniqueness of the steady state solution, this confirms the inadequacy of such a boundary condition to simulate actual melting furnaces for which two recirculation loops are required to obtained good glass quality. The flow under the batch is similar to that of the baseline case, i.e., sixteen cells develop in the spanwise direction. It indicates that the flow structure under the batch in the spanwise direction is not significantly affected by the heat flux distribution in the longitudinal direction even though it drives the molten glass from the hot spot towards the batch. Indeed, the cells forming under the batch are due to temperature gradients in the lateral direction that strongly depend on the heat losses throughthe sidewalls but not on the heat flux distribution from the combustion space to the glass bath.
Figure 8 shows the streamtraces at x = 15 m in the case of a uniform heat flux distribution. It must be compared with Figure 6 at the same cross-section. One can see that the two cells forming at the surface in the baseline case do not form when a uniform heat flux is imposed. It shows that the cooling of the sidewalls alone is not responsible for the formation of the cells. Instead, the negative heat flux uniform across the width combined the heat losses through the sidewalls cause the cells to form preferentially close to the sidewalls due to greater temperature gradient in the vicinity of the sidewalls.

Effect of the Location of the Zero Heat Flux L_0

Depending on the furnace design and on the firing pattern, the net heat flux distribution from the combustion space to the glass melt can be affected substantially. For example, in the presence of an exhaust at the end of the furnace combined with a firing pattern centered in the first half of the furnace, the zone of negative heat flux from the combustion space to the glass melt can be large. The extent of this region is characterized by the location of the zero heat flux L_0. In the present study, L_0 was taken as 12.84 m, 13.84 m (baseline case), and 15.84 m.

The major effects of the location of the zero heat flux L_0 on the flow pattern can be seen in the longitudinal direction. Figure 9 compares the streamtraces at the centerline for the three values of L_0. One can see that the extent of the second recirculation loop increases significantly as the location of the zero heat flux is shifted toward the center of the tank. By reducing the first circulation loop, one confines the unmelted sand grains and the gas bubbles in the first half of the tank away from the throat. This allows more time for the refining and melting processes to take place.

Effect of the Location of the Maximum Heat Flux L_{max}

In a manner similar to that used for the location of the zero heat flux, the location of the maximum heat flux was changed around the baseline value of 7.5 m. Three different locations were studied, L_{max} = 6.5 m, 7.5 m, and 8.5 m. Figure 10 shows that the flow pattern is not significantly affected by the change in the location of the maximum heat flux. In the present cases, the gradient of the heat flux in the x-direction is only slightly modified by the change in L_{max} from 6.5 m to 8.5 m, as shown in Table 1 and therefore does not affect the flow significantly.

Effect of the Presence of Foam

A fraction of the bubbles that are generated by the fusion of raw materials in the batch and by the fining reactions in the melt accumulate on the free surface of the glass to produce the primary foam [27]. Resorption of the remaining small gas bubbles, taking place during the conditioning of the glass melt as it flows from the hot spot in the middle of the bath towards the throat of the furnace, also leads to formation of the so-called

secondary foam [27]. Visual observations and laboratory scale studies of furnace operations indicate that the foam layers of various thickness can cover a large fraction of the free surface of the molten glass [27]. Since the foam is an inhomogeneous medium, it acts essentially as a collection of radiation scatterers, and, therefore, provides significant resistance to heat transfer by radiation from the combustion space to the molten glass [35–37]. Indeed, according to Trier [35], this resistance could lead to a decrease by as much as 60% in the radiative fluxes at the glass/combustion space interface.

In the present study, the foam was assumed to cover roughly the second third of the tank surface, i.e., from x = 6.5 m to 11.25 m. The net heat flux from the combustion space to the glass melt was reduced by 50 % in this region compared to the baseline case. Figure 11 shows the velocity, temperature fields as well as the streamtraces. It is clear that foam has a strong impact on the flow and temperature field. In particular, the temperature of the glass melt is significantly reduced by the presence of the foam. The reduction of glass melt temperature is probably responsible for the third recirculation loop forming under the batch close to the back wall. Indeed, the axial velocity of the batch combined with the exponential increase of the glass melt viscosity with the decreasing temperature are responsible for the large shear stress at the batch/glass melt interface that propagates deeper in the glass melt and generate a cell that expand across the tank in the lateral direction. Moreover, the lateral flow under the batch and under the foam is not significantly different from that of the baseline case.

Effect of the Shape of the Heat Flux in the Spanwise Direction

So far, the heat flux distribution in the spanwise direction was taken as uniform. In reality, however, due to the cooling of the walls in the combustion space and to the flame shape, the heat flux from the combustion space to the glass melt should be reduced close to the sidewalls and have a maximum near the centerline. The effect of the heat flux distribution in the spanwise direction was studied by introducing a dimensionless multiplying function $q^*(y)$ to the heat flux $q''(x)$ while keeping the overall heat input rate from the combustion space constant at 8.3 MW. The lateral heat flux distribution $q^*(y)$ was assumed to take a top hat-shape (simulations 7) or a parabolic shape (simulations 8) as shown in Figure 12.

The changes in the heat flux distribution in the spanwise direction do not affect significantly the flow and temperature pattern under the batch, close the the front wall or at the center line. In these regions, the cooling of the sidewalls combined with the constant temperature under the batch and the cooling of the front wall, respectively, dominate the heat transfer and thus, the natural convection flow. There, the effect of the non-uniformity of the heat flux distribution in the spanwise direction is negligible. In the center of the tank for $7m < x < 13m$, however, four cells form in each corner of the cross-section instead of two in the bottom corners for the baseline case as shown in Figure 13. This tend to show that the cells forming in the spanwise direction are due to the gradient of temperature in the y-direction.

CONCLUSIONS

This paper presents a systematic parametric study of the flow pattern in a model glass melting furnace with a throat. The main purpose is to evaluate the capability of the furnace operators to control the glass flow and temperature fields by adjusting the firing in the combustion space. In particular, the effects of the following parameters are discussed: (i) the uniform heat flux distribution, (ii) the location of the zero heat flux L_0, (iii) the location of the maximum heat flux L_{max}, (iv) of the shape of the heat flux in the spanwise direction. The total heat input is 8.3 MW in all the simulations and the qualitative analysis presented leads to the following conclusions:

1. The flow pattern observed by Zhiqiang and Zhihao [1] in the longitudinal direction and represented in Figure 2 is confirmed. A part of the pull current flows directly from under the batch to the throat. Such a flow pattern tends to deteriorate the glass quality since unmelted sand grains and bubbles generated under the batch may not have enough time to melt or rise at the surface and may end up in the final product.

2. A heat flux gradient in the x-direction is required to generate two recirculation loops in the longitudinal direction.

3. A steep heat flux gradient in the refining part of the tank increase significantly the size of the second recirculation loop. In our simulations, the steepest heat flux gradient is obtained by modifying the location of the zero heat flux.

4. The change of the heat flux distribution has no appreciable effect on the flow pattern under the batch blanket. Sixteen cells develop under the entire length of the batch but the cells disappear in part of the tank where the glass is free of the batch.

5. The negative heat flux from the combustion space to the glass melt (i.e., heat loss from the glass melt to combustion space) causes two cells to form in the lateral direction, at the surface of the glass melt, and close to the front wall.

6. A nonuniform heat flux distribution in the spanwise direction causes two cells to form at the glass melt surface near the side walls.

References

[1] Y. Zhiqiang and Z. Zhihao, "Basic flow pattern and its variation in different types of glass tank furnaces", *Glastechnische Berichte*, vol. 70, pp. 165–172, 1997.

[2] R. Viskanta, "Review of three-dimensional mathematical modeling of glass melting", *Journal of Non-Crystalline Solids*, vol. 177, pp. 347–362, 1994.

[3] M. Cable, "A century of developments in glassmelting research", *Journal of the American Ceramic Society*, vol. 81, pp. 1083–1091, 1998.

[4] K-O Lim, K-S Lee, and T-H Song, "Primary and secondary instabilities in a glass-melting surface", *Numerical Heat Transfer, Part A*, vol. 36, pp. 309–325, 1999.

[5] K-O Lim, T-H Song, and K-S Lee, "Pattern of natural convection driven by the free surface temperature distribution in a glass melting furnace", *Glass Technology*, vol. 39, pp. 27–31, 1998.

[6] W. Jian and Z. Zhihao, "Investigation into glass tank geometries by means of a mathematical model", *Glastechnische Berichte*, vol. 65, pp. 1–8, 1992.

[7] G. Zhao, Z. Guo, and W. Hu, "Quantitative evaluation for glass fusion processes", in *Proceedings of the XVII International Congress on Glass*, Beijing, P. R. China, 1995, Chinese Ceramic Society, vol. 6, pp. 380–385.

[8] N. W. E. Curlet, K. J. Won, L. A. Clomberg Jr., and A. F. Sarofim, "Experimental and mathematical modeling of three-dimensional natural convection in an enclosure", *AIChE Journal*, pp. 249–257, 30, No. 2.

[9] A. Ungan and R. Viskanta, "Three-dimensional numerical modeling of circulation and heat transfer in a glass melting tank. Part. 2 sample simulations", *Glastechnische Berichte*, vol. 60, No.4, pp. 115–124, 1987.

[10] A. Ungan and R. Viskanta, "Identification of the structure of the three dimensional thermal flow in an idling container glass melter", *Glass Technology*, vol. 28, No. 6, pp. 252–260, 1987.

[11] A. Ungan and R. Viskanta, "Three-dimensional numerical modeling of circulation and heat transfer in a glass melting tank. Part. 1 mathematical formulation", *Glastechnische Berichte*, vol. 60, No.3, pp. 71–78, 1987.

[12] J. Wang, B. S. Brewster, M. Q. McQuay, and B. W. Webb, "Validation of an improved batch model in a coupled combustion space/melt tank/batch melting glass furnace simulation", *Glastechnische Berichte*, vol. 73, No. 10, pp. 299–308, 2000.

[13] S. Kawachi and Y. Kawase, "Evaluation of bubble removing performance in a TV glass furnace. Part 1. mathematical formulation", *Glastechnische Berichte*, vol. 71, No.4, pp. 83–91, 1998.

[14] S. Kawachi and Y. Kawase, "Evaluation of bubble removing performance in a TV glass furnace. Part 2. verification using real furnace data", *Glastechnische Berichte*, vol. 71, No.5, pp. 111–119, 1998.

[15] R. R. Hayes, J. Wang, M. Q. McQuay, B. W. Webb, and A. M. Huber, "Predicted and measured glass surface temperatures in an industrial regenerative gas-fired, flat glass furnace", *Glastechnische Berichte*, vol. 72, pp. 367–377, 1999.

[16] K.-B. Cheong, K.-M Moon, and T.-H. Song, "Treatement of radiative transfer in glass melts: validity of Rosseland and P-1 approxiamtions", *Physics and Chemistry of Glasses*, vol. 40 No.1, pp. 26–33, 1999.

[17] M. K. Choudhary, "Three-dimensional mathematical model for flow and heat transfer in electric glass furnaces", *Heat Transfer Engineering*, vol. 6, No. 4, pp. 55–65, 1985.

[18] A. Ungan and R. Viskanta, "Melting behavior of continuously charged loose batch blankets in glass melting furnaces", *Glastechnische Berichte*, vol. 59, No.10, pp. 279–291, 1986.

[19] S. Patankar, *Numerical heat transfer and fluid flow*, Hemisphere, Washington, DC, 1980.

[20] R. G. C Beerkens and H. De Wall, "Mechanism of oxygen diffusion in glassmelts containing variable-valence ions", *Journal of the American Ceramic Society*, vol. 73, No.7, pp. 1857–1861, 1990.

[21] M. K. Choudhary and N. T. Huff, "Mathematical modeling in the glass industry: an overview of status and needs", *Glastechnische Berichte*, vol. 70, pp. 363–370, 1997.

[22] R. H. Doremus, *Glass science*, John Wiley & Sons, New York, NY, 1994.

[23] C. L. Babcock, *Silicate glass technology methods*, John Wiley & Sons, New York, 1977.

[24] H. Scholze, *Glass nature, structure and properties, 3rd. Edition*, Springer-Verlag, Berlin, 1991.

[25] M. Coenen, "Dichte von ,,schlierengläsern bei hohen temperaturen", *Glastechnische Berichte*, vol. 39, pp. 81–89, 1966.

[26] T. Lakatos, L.-G. Johansson, and B. Simmingsköld, "Viscosity temperature relations in the glass system SiO_2-Al_2O_3-Na_2O-K_2O-CaO-MgO in the composition range of technical glasses.", *Glass Technology*, vol. 13, pp. 88–95, 1972.

[27] P. R. Laimbock, *Foaming of glass melts*, PhD thesis, Technical University of Eindhoven, Eindhoven, The Netherlands, 1998.

[28] M. Ishii and T. C. Chawla, "Local drag laws in dispersed two-pahse flow", ANL-79-105, NUREG/CR-1230, 1979.

[29] D. E. Sharp and L. B. Ginther, "Effect of composition and temperature on the specific heat of glass", *Journal of the American Ceramic Society*, vol. 34, pp. 260–271, 1951.

[30] C. L. Babcock and D. L. McGraw, "Controlling conductivity in silicates", *Glass Industry*, vol. 38, pp. 147–151, 1957.

[31] A. F. Van Zee and C. L. Babcock, "A method for the measurement of thermal diffusivity of molten glass", *Journal of the American Ceramic Society*, pp. 244–250, 1951.

[32] C. Madivate, F. Müller, and W. Wilsmann, "Calculation of the theoretical energy requirement for melting technical silicate glasses", *Journal of the American Ceramic Society*, vol. 81, pp. 3300–3306, 1998.

[33] C. Madivate, "Calculation of the theoretical energy requirement for melting technical silicate glasses", *Journal of the American Ceramic Society*, vol. 81, pp. 3300–3306, 1998.

[34] J. Shell, "Temperature measurements in the Techneglas Furnace C", Personal Communications, May, 1998.

[35] W. Trier, "Wärmeübergang zwischen Flamme and Glasbad Glasschmelzwannenofen", *Glastechnische Berichte*, vol. 36, No.3, pp. 73–86, 1963.

[36] A. G. Fedorov and R. Viskanta, "Radiative transfer in a semitransparent glass foam blanket", *Physics and Chemistry of Glasses*, vol. 41 No.3, pp. 127–135, 2000.

[37] A. G. Fedorov and R. Viskanta, "Radiative characteristics of glass foams", *Journal of the American Ceramic Society*, vol. 83 No.11, pp. 2769–2776, 2000.

Figure Captions

Figure 1. *Schematic of the ideal flow pattern furnaces with a throat.*

Figure 2. *Schematic of the flow pattern observed by zhiqiang and Zhihao (1997) in furnaces with a throat.*

Figure 3. *Schematic of the modelled glass melting tank and its system of coordinates.*

Figure 4. *Heat flux distribution used as the boundary condition at the glass melt/combustion space interface.*

Figure 5. *From top to bottom (a) velocity field, (b) temperature field, and (c) streamtraces at the tank centerline for the baseline case.*

Figure 6. *Streamlines in the spanwise direction for the baseline case for (from top to bottom) (a) x = 3.5 m, (b) x = 7 m, (c) x = 10 m, (d) x=13 m, (e) x=14 m, and (f) x = 15 m.*

Figure 7. *From top to bottom (a) velocity field, (b) temperature field, and (c) streamtraces at the tank centerline.*

Figure 8. *Streamlines at x = 15 m for a uniform heat flux distribution.*

Figure 9. *Effect of L_0 on the streamtraces at the centerline for (from top to bottom) (a) L_0 = 12.84 m, (b) L_0 = 13.84 m, and (c) L_0 = 15.84 m.*

Figure 10. *Effect of L_{max} on the streamtraces at the centerline for (from top to bottom) (a) L_{max} = 6.5 m, (b) L_{max} = 7.5 m, and (c) L_0 = 8.5 m*

Figure 11. *Effect of the presence of foam on (a) the velocity field, (b) the temperature field, and (c) the streamtraces at the tank centerline.*

Figure 12. *Heat flux distribution in the spanwise direction used as the boundary condition at the glass melt/combustion space interface.*

Figure 13. *Comparison of the streamtraces at the cross-section x = 10 m for the baseline case and non-uniform heat flux distribution in the spanwise direction (simulations 7 and 8)*

Table Captions

Table 1. *Summary of the parameters used in the three-dimensional simulation.*

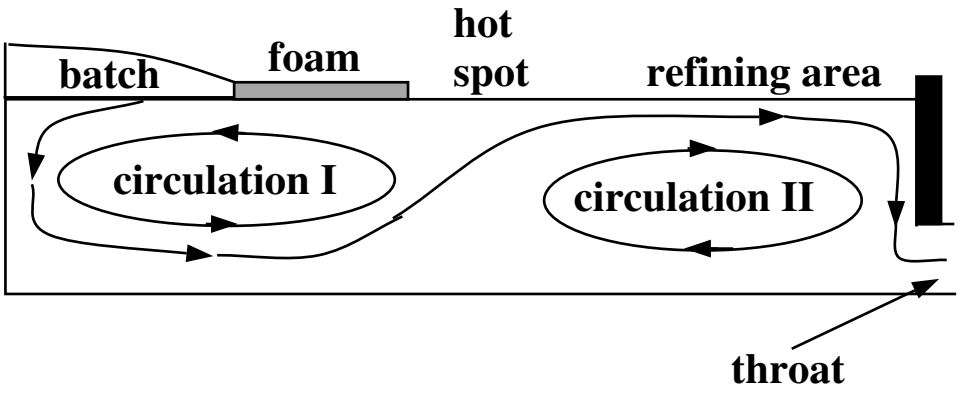

Figure 1: *Schematic of the ideal flow pattern furnaces with a throat.*

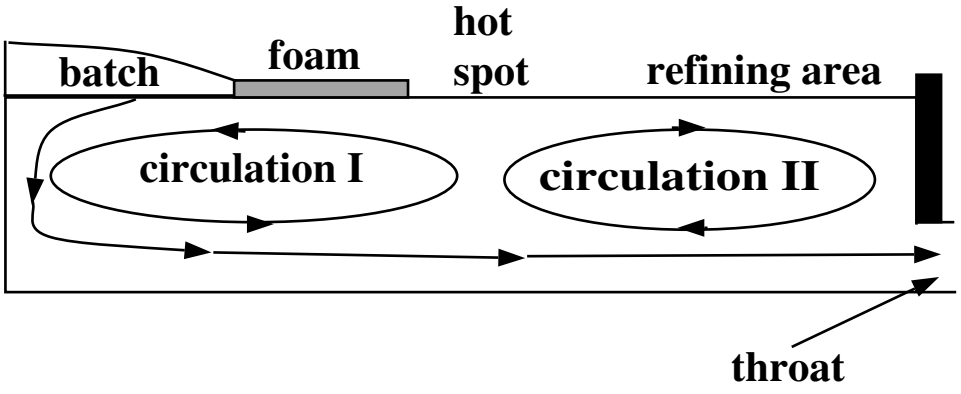

Figure 2: *Schematic of the flow pattern observed by zhiqiang and Zhihao (1997) in furnaces with a throat.*

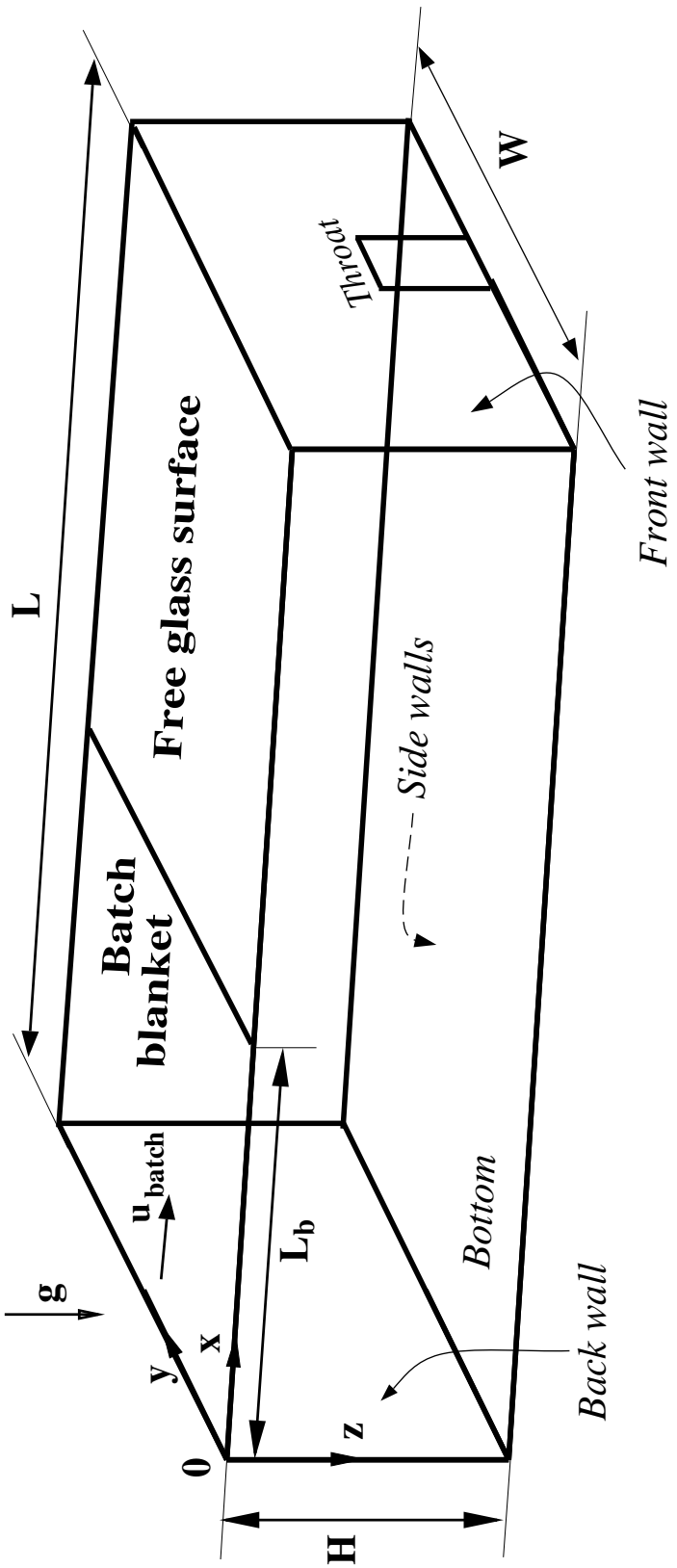

Figure 3: *Schematic of the modelled glass melting tank and its system of coordinates.*

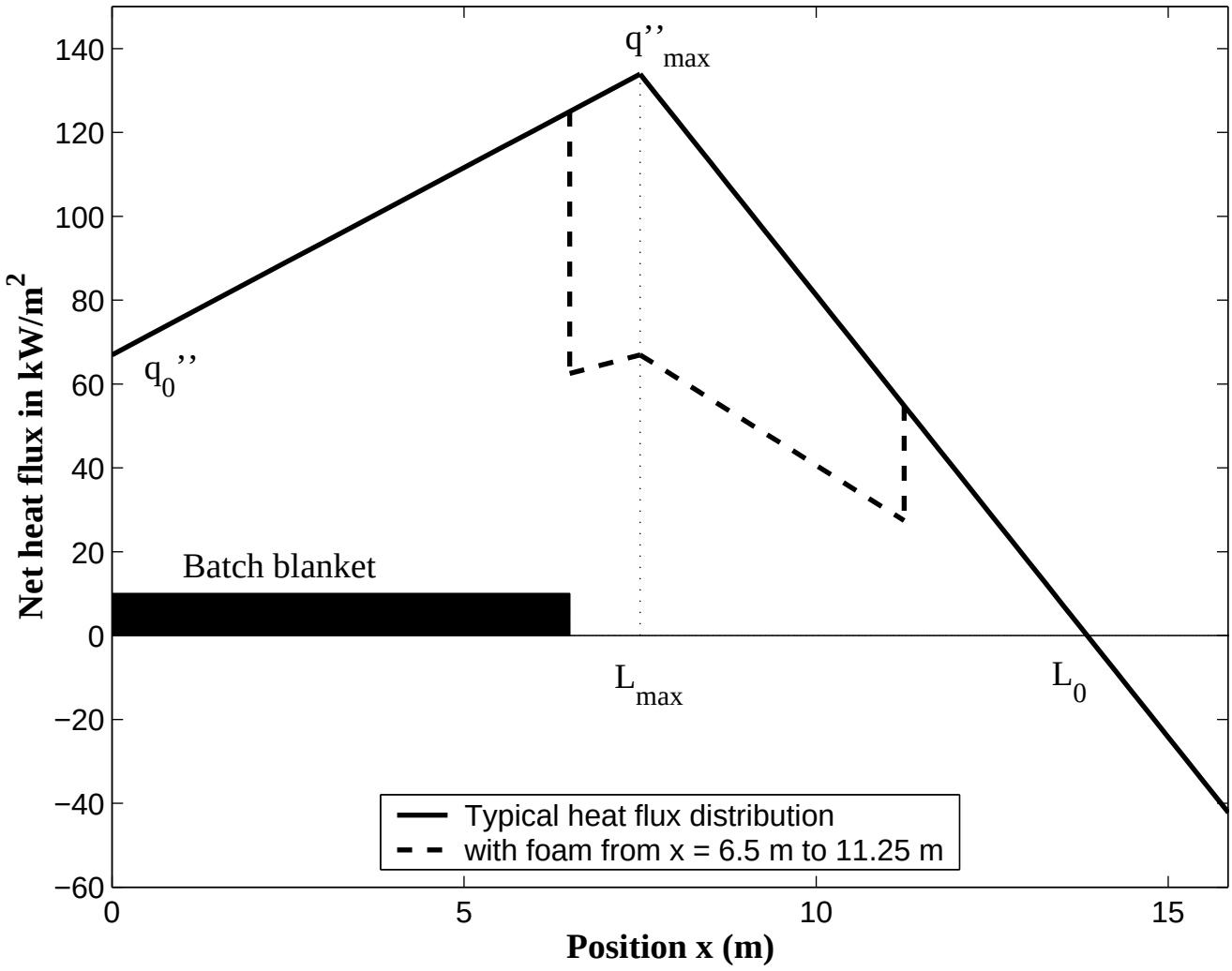

Figure 4: *Heat flux distribution used as the boundary condition at the glass melt/combustion space interface.*

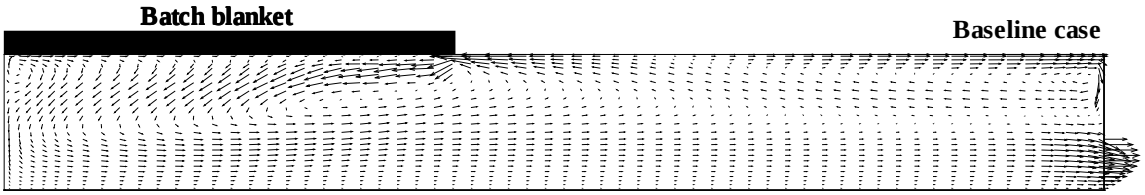

(a)

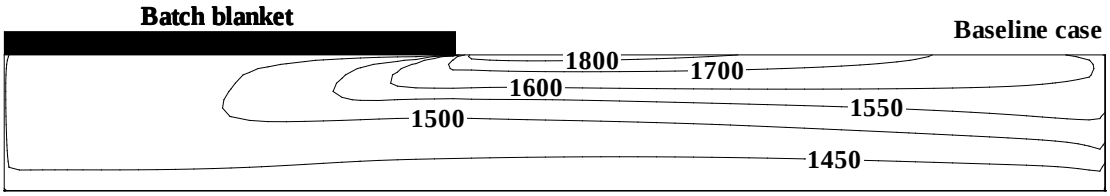

(b)

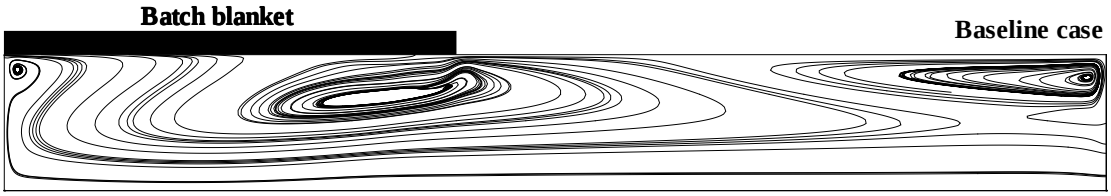

(c)

Figure 5: *From top to bottom (a) velocity field, (b) temperature field, and (c) streamtraces at the tank centerline for the baseline case.*

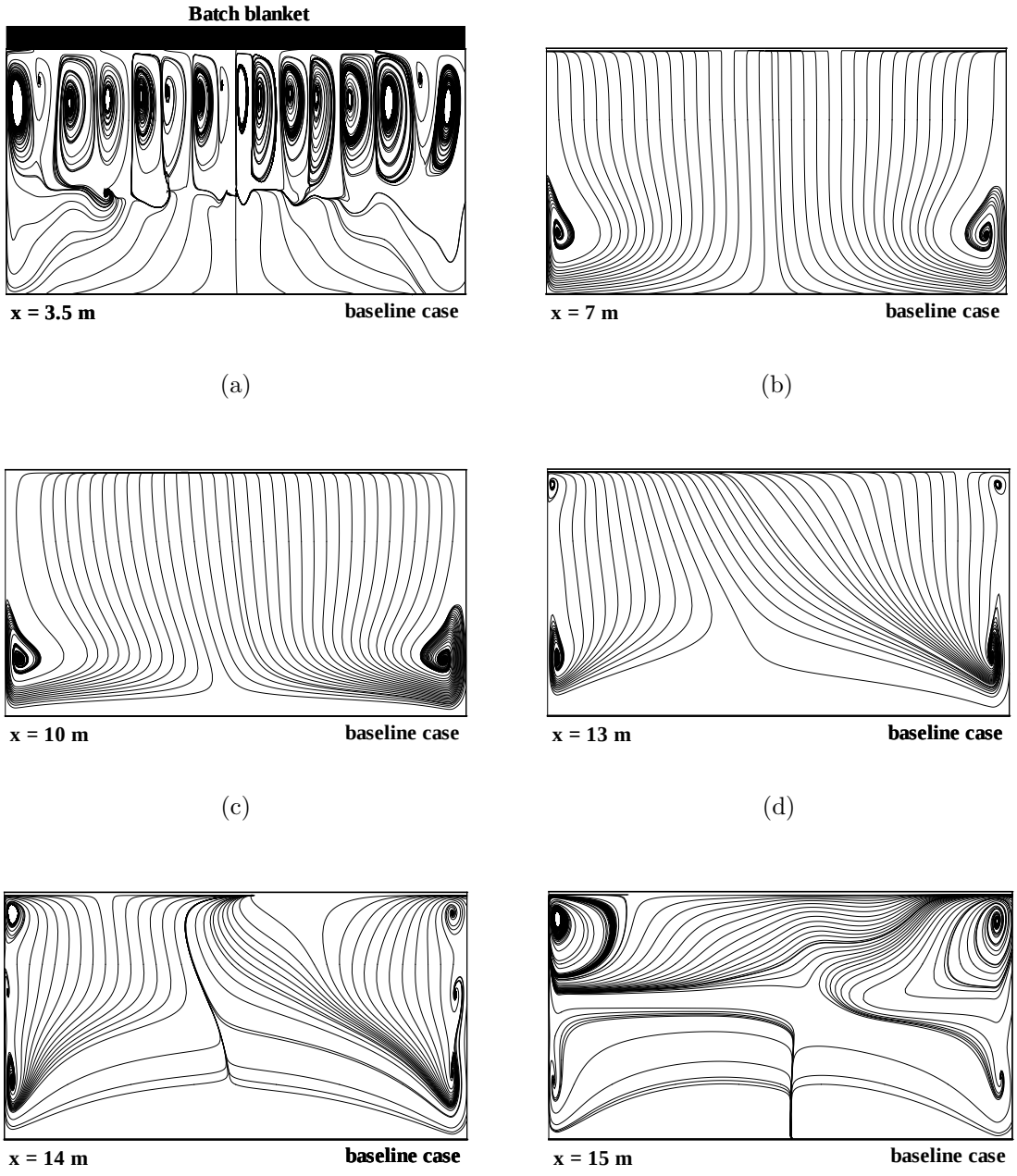

Figure 6: *Streamlines in the spanwise direction for the baseline case for (from top to bottom) (a) x = 3.5 m, (b) x = 7 m, (c) x = 10 m, (d) x=13 m, (e) x=14 m, and (f) x = 15 m.*

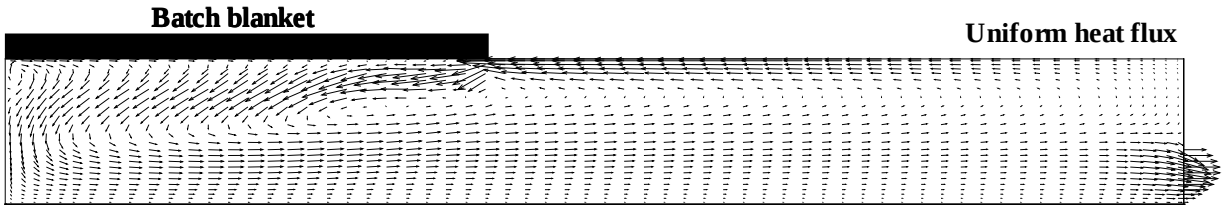

(a)

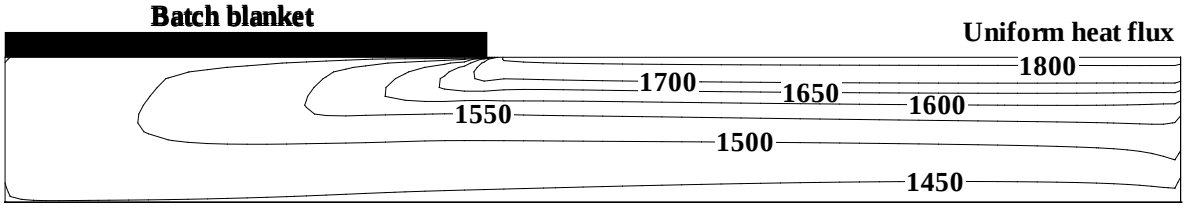

(b)

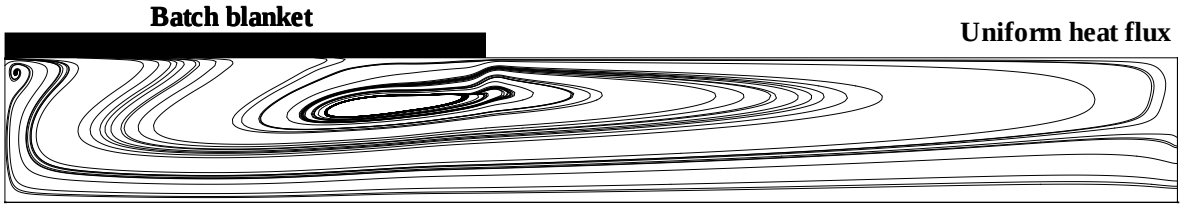

(c)

Figure 7: *From top to bottom (a) velocity field, (b) temperature field, and (c) streamtraces at the tank centerline.*

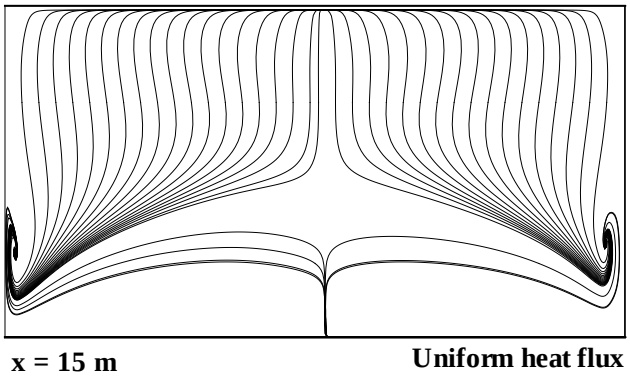

Figure 8: *Streamlines at $x = 15$ m for a uniform heat flux distribution.*

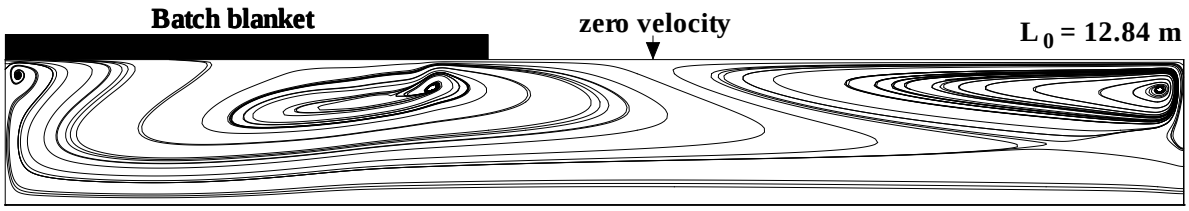

(a)

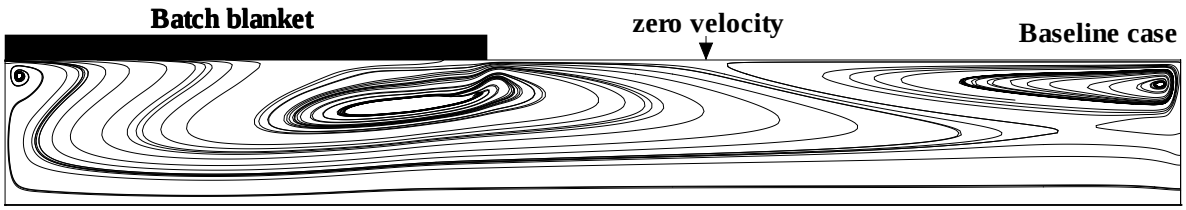

(b)

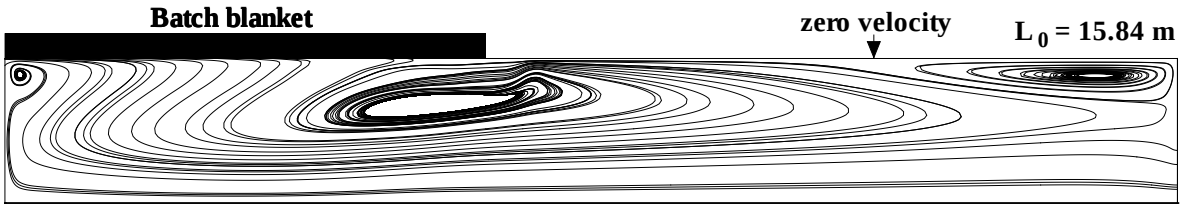

(c)

Figure 9: *Effect of L_0 on the streamtraces at the centerline for (from top to bottom) (a) L_0 = 12.84 m, (b) L_0 = 13.84 m, and (c) L_0 = 15.84 m.*

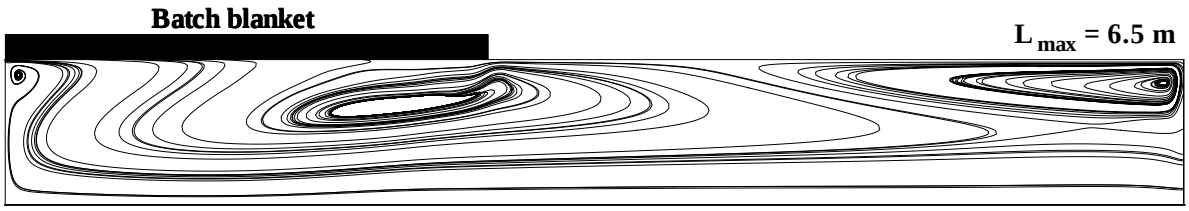

(a)

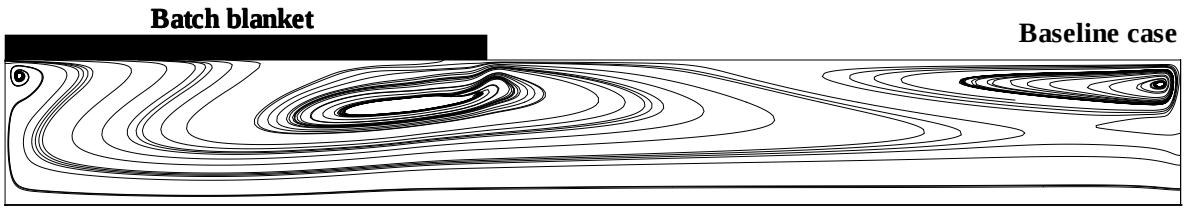

(b)

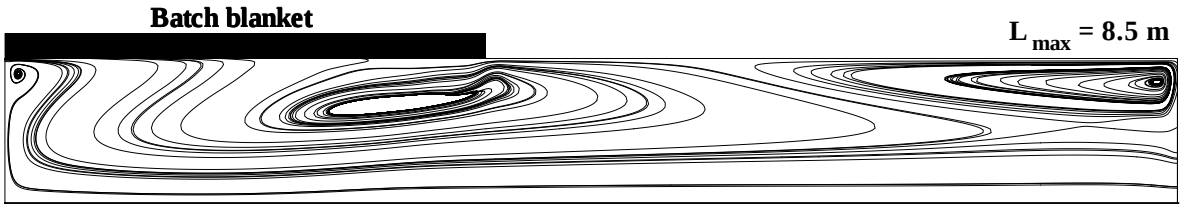

(c)

Figure 10: *Effect of L_{max} on the streamtraces at the centerline for (from top to bottom) (a) L_{max} = 6.5 m, (b) L_{max} = 7.5 m, and (c) L_0 = 8.5 m*

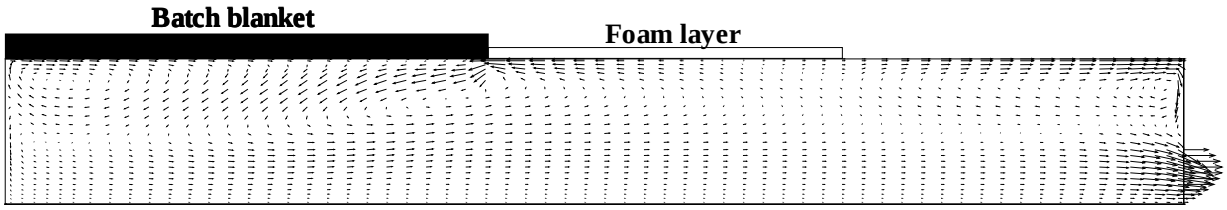

(a)

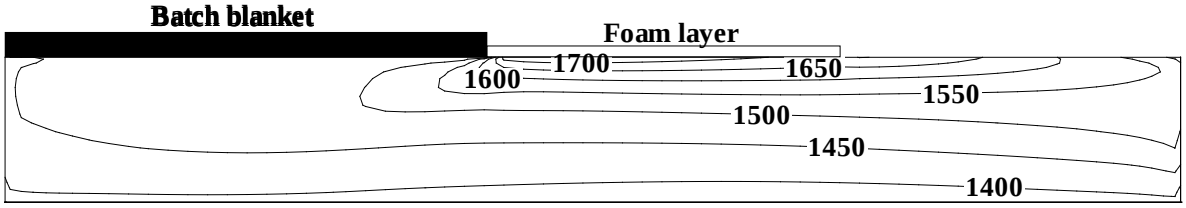

(b)

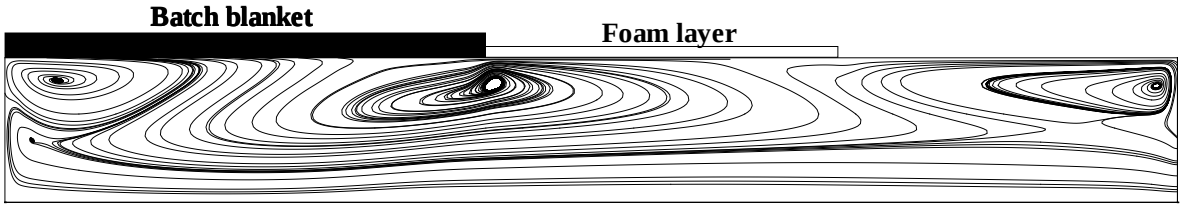

(c)

Figure 11: *Effect of the presence of foam on (a) the velocity field, (b) the temperature field, and (c) the streamtraces at the tank centerline.*

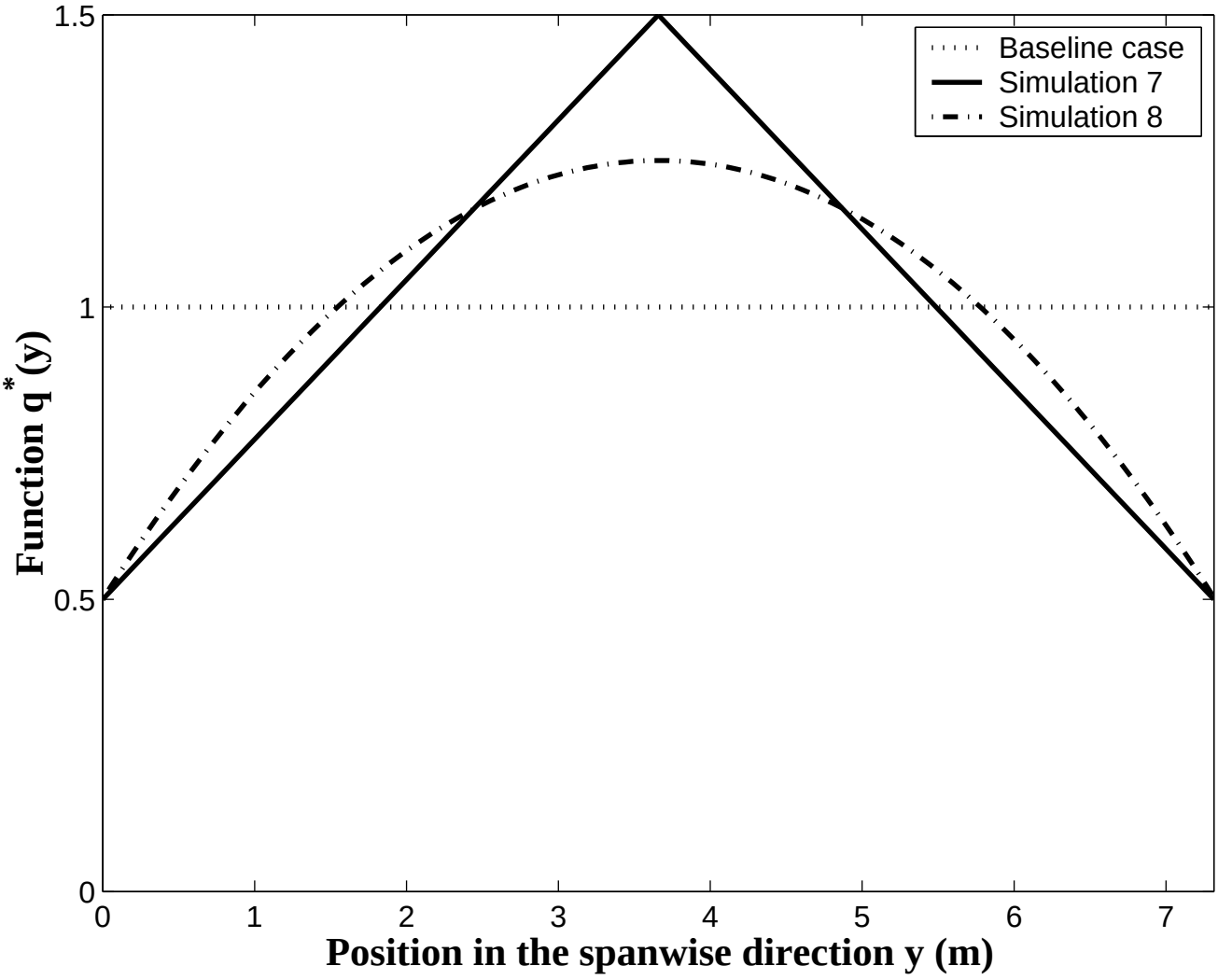

Figure 12: *Heat flux distribution in the spanwise direction used as the boundary condition at the glass melt/combustion space interface.*

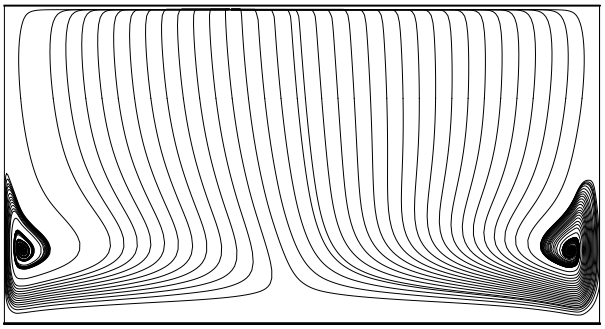

x = 10 m **baseline case**

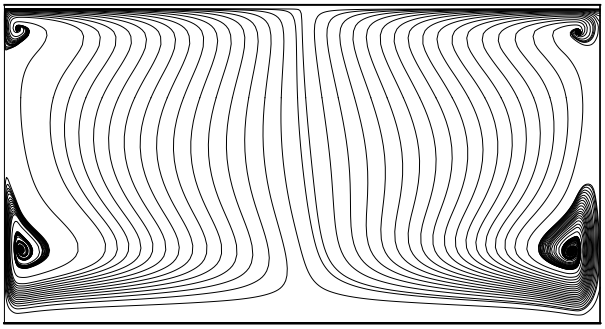

x = 10 m **simulation 7**

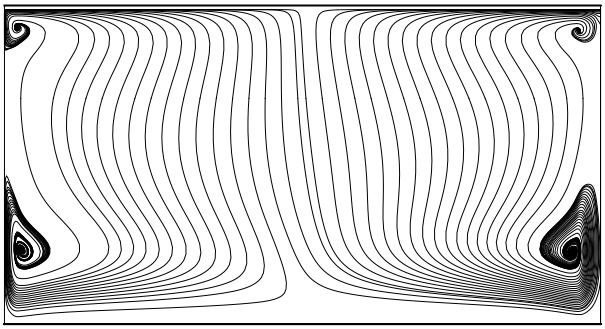

x = 10 m **simulation 8**

Figure 13: *Comparison of the streamtraces at the cross-section x = 10 m for the baseline case and non-uniform heat flux distribution in the spanwise direction (simulations 7 and 8)*

Table 1: *Summary of the parameters used in the three-dimensional simulation.*

Simulation	**q"$_{max}$** **(kW/m^{2}K)**	**q"$_0$** **(kW/m^{2}K)**	**L$_0$** **(m)**	**L$_{max}$** **(m)**	**q*(y)**	**L$_{batch}$** **(m)**	**Foam**	$\frac{\partial q''(x,y)}{\partial x}\Big\|_{x \geqslant L_{max}}$ **(kW/m^{3}K)**
Baseline case	133.92	q"$_{max}$/2	13.84	7.5	1.0	6.5	no	-21.1
1 [q"(x) = Constant]	71.65	q"$_{max}$	-	-	1.0	6.5	no	0
2	140.65	2q"$_{max}$/3	**12.84**	7.5	1.0	5.92	no	-26.3
3	115.94	q"$_{max}$/2	**15.84**	7.5	1.0	7.01	no	-13.9
4	133.92	q"$_{max}$/2	13.84	7.5	1.0	6.5	yes	-10.6
5	133.92	q"$_{max}$/2	13.84	**6.5**	1.0	6.5	no	-18.2
6	133.92	q"$_{max}$/2	13.84	**8.5**	1.0	6.5	no	-25.1
7	133.92	q"$_{max}$/2	13.84	7.5	**Hat**	6.5	no	-21.1
8	133.92	q"$_{max}$/2	13.84	7.5	**Parabolic**	6.5	no	-21.1